[redacted]

NRL REPORT 3690

TRANSPARENCY OF AN ACID-ANILINE FLAME TO S-BAND RADIATION

H. M. Bryant and D. L. Fye

June 23, 1950

Approved by:

Mr. F. M. Gager, Head, Special Research Branch
Dr. R. M. Page, Superintendent, Radio Division III

NAVAL RESEARCH LABORATORY
CAPTAIN F. R. FURTH, USN, DIRECTOR
WASHINGTON, D.C.

[redacted]

DISTRIBUTION

CNO	1
ONR	
Attn: Code 470	1
Dir., USNEL	2
CDR, USNOTS	
Attn: Reports Unit	2
CO, USNAD, Dover, N. J.	1
Wright-Patterson AFB	
Attn: BAU-CADO	1
Attn: CADO-E1	2
Attn: Ch., Electronics Subdiv., MCREEO-2	1
CO, AMC, Watson Labs, Red Bank	
Attn: ENR	1
CO, Air Force Cambridge Res. Labs.,	
Attn: ERRS	1
OCSigO	
Attn: Ch. Eng. & Tech. Div., SIGTM-S	1
CO, SCEL	
Attn: Dir. of Eng.	2
Dir., NBS	
Attn: CRPL	1
RDB	
Attn: Information Requirements Branch	2
Attn: Navy Secretary	1
Naval Res. Sec., Science Div., Library of Congress	
Attn: Mr. J. H. Heald	2

ANAF-G/M Mailing List No. 11
Parts A, C, DG, and DP

[redacted]

CONTENTS

[redacted]

ABSTRACT

The reaction-motor flames of the "Lark" Missile were checked in static thrust for effective transmission of S-band radiation. Statistical averages, presented in the form of percent deviation from the normal amplitude of a transmitted signal, indicate that these flames are nearly transparent to the S-band radiation. The slight effects of such variables as plane of polarization, portion of the flame penetrated, and change in carrier frequency were considered.

PROBLEM STATUS

This is the fifth in a series of interim reports on the general problem of propagation through propellant gasses; work is continuing.

AUTHORIZATION

NRL Problem R11-13R
NR 511-130

[redacted]

TRANSPARENCY OF AN ACID-ANILINE FLAME TO S-BAND RADIATION

INTRODUCTION

This report is the fifth in a series emanating from Radio Division III, Naval Research Laboratory, covering various phases of activity on "Radio Wave Propagation Through Propellant Gases." It is suggested that the reader consult previous reports in this series to obtain the necessary background.[1,2,3,4] A general discussion by Gager[1] of activity on the problem presents theoretical background and serves as an over-all introduction to any subsequent reports covering individual phases of the problem. A report by Gager, et al.[2] is concerned with S-band transmission through the "Lark" acid-aniline flames. This propagation study is restricted to horizontal polarization and discusses in detail certain experimental field techniques which were adapted to the motor performance facilities of Reaction Motors, Inc., Lake Denmark (Dover), New Jersey. Gager, et al.[3] discuss measuring techniques and data analysis of an incidental modulation study of an S-band transmission circuit with interposed "Lark" acid-aniline flames. Vibration effects, light intensity variations, and sound intensity variation associated with the flames are also treated.

The present study included a statistical analysis of further S-band propagation data, using the "Lark" Missile flames. The secondary effects due to polarization plane, frequency shift, and displacement of the point of impingement of radiation on the flame were investigated, and results obtained represent the most probable values superimposed on an error envelope designating the area in which the true values should be contained.

EXPERIMENTAL ARRANGEMENT

Motors and Fuel

The acid-aniline reaction motors employed were the 400- and 220-pound-thrust units manufactured by Reaction Motors, Inc., for use in the "Lark" Missile. The motors were mounted on a horizontal thrust stand, the small motor above the large one, with the large motor throat approximately 27 inches from the ground (Figures 1 and 2). The motors were fueled with mixed-acid and aniline for all firings. The mixed-acid was a commercial product (88 percent nitric and 12 percent sulphuric); the aniline (commercial

---

[1]Gager, F. M., "Propagation of Electromagnetic Waves Through Propellant Gases," NRL Report R-3197 ([redacted]), November 1947

[2]Gager, F. M., Zettle, E. N., Bryant, H. M., and Boyd, F. E., "S-Band Propagation with Acid-Aniline Flame Barriers," NRL Report R-3209 ([redacted]), December 1947

[3]Gager, F. M., Grimm, H. H., Peck, R. C., and Morehouse, G. D., "Incidental Flame Modulation of S-Band Continuous Wave Radiation," NRL Report No. R-3261 ([redacted]), March 1948

[4]Gager, F. M. and Schleter, G. C., "Electromagnetic Probes for Supersonic Flames," NRL Report 3505 ([redacted]), June 1949 (Number four in the series)

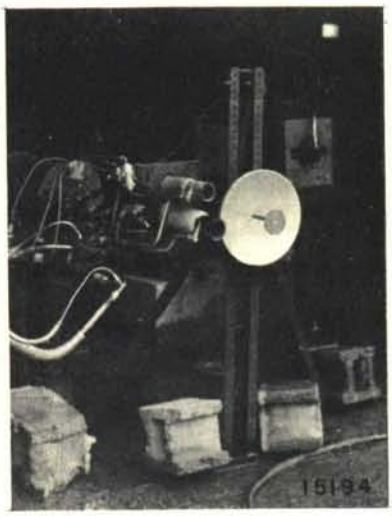

Figure 1 - Motors mounted on static thrust stand; transmitting antenna in position B

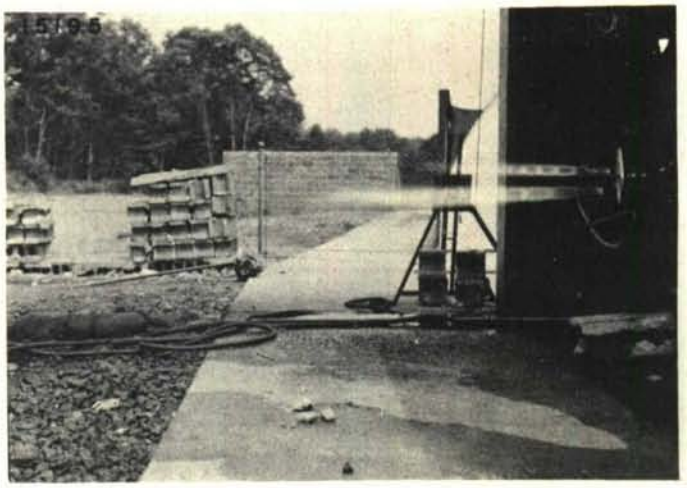

Figure 2 - Both motors firing; transmitting antenna in position B

grade) was supplied to Reaction Motors, Inc., by the Fuels and Lubrication Section, Bureau of Aeronautics. Repeatable performances of the motor flames were possible since each successive run of the reaction motors was made under fuel pressurizing conditions as nearly constant as were obtainable.

Instrumentation

From information received on a previous field trip[5] and other considerations, it was decided that data should be obtained to show, under various conditions of single- and two-motor operation: (a) The slight effects of polarization (vertical vs. horizontal), (b) shifting of the frequency, (c) adjustment of the incident angle of impinging radiation, and (d) changing of the points of incidence upon the flame. Furthermore, it was decided that the performance of the measuring system should be observed under several types of inactive barriers (conductor, nonconductor, etc.) other than the flame. The same S-band transmitter, dipole pick-up probe assemblies, and antenna stands were used as on the previous field trip.

An arc of dipole pick-ups (Figure 3) was employed to indicate any changes in the distribution, (due to the interposition of a barrier), of transmitted energy, the frequency of which was monitored with a Sperry Type MK-S21 Detector-Wavemeter. A "disk and dish" reflector (Figure 1) was used with the transmitting dipole to confine and direct the transmitted energy from a 10-watt c-w magnetron source upon the flame or flames. The transmitting antenna polar pattern (quasi free-space) is shown superimposed upon the physical arrangement of the transmitting and receiving dipoles (Figure 4). This general measurement technique provided for the interposition of the flame or flames in the multiple transmission paths from the transmitting antenna to the pick-up dipoles and allowed a ready change in the main lines of incidence. All the data presented in this

[5] op. cit., Gager, F. M., Zettle, E. N., Bryant, H. M., and Boyd, F. E.

Figure 3 - Arc of pick-up dipoles with associated reflectors and stands

report was taken with the arc of pick-up dipoles located in the horizontal plane through the center of the throat of the 400-pound thrust motor.

Each pick-up dipole (Figure 3) was provided with a special choke-type crystal holder mounted immediately behind the one-foot-square backplate and contained a Type 1N21B crystal rectifier. The rectified r-f currents from these crystals were conducted through shielded cables to a remote bank of Esterline-Angus recorders (Type AW, 1 ma scale) (Figure 5) which recorded the actual crystal currents.

The block diagram (Figure 6) illustrates the instrumentation arrangement used in obtaining the data presented in this report. The angular displacement and linear distances between the transmitting and pick-up dipoles can be obtained from the plan view (Figure 4), which is drawn to scale.

DATA OBTAINED

An extensive series of measurement runs were made in order to better separate the variables under consideration (frequency, angle of incidence, polarization, etc.). Each figure in this report showing single-case or combined flame-barrier data carries the associated test-run numbers. Where data is of a combined nature, it should be realized that the runs are being treated together statistically (see Appendix). For convenience, a table showing the experimental conditions under which some of the pertinent flame-barrier runs were made is included (Table 1).

TREATMENT OF DATA

The material presented in this report is an analysis of the amplitude behavior of the rectified r-f currents from the crystals mounted behind the pick-up dipoles. Typical sections of a record taken from one of the Esterline-Angus recorders are shown (Figure 7). The notched line on the right margin of the chart is a time record from an electronic timer used to provide synchronized reference points for comparing data from the several charts.

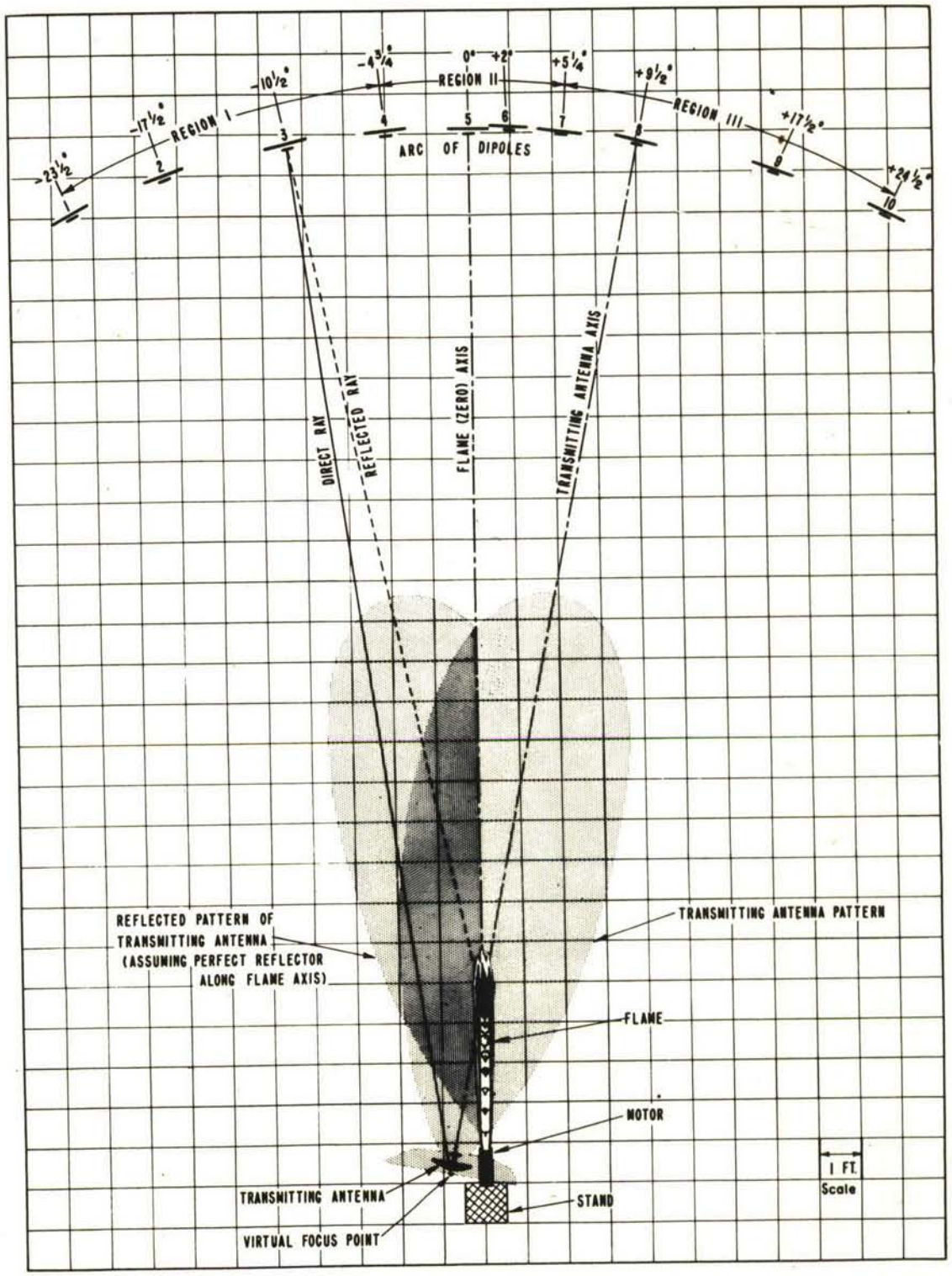

Figure 4 - Diagram (to scale) showing arrangement of propagation

[redacted]

Table 1

Pertinent Test Runs*
Dish Transmitting Antenna Aimed at Pick-Up No. 8

Run No.	Polarization	Antenna Aim	Frequency (Mc)	Motor	Pounds Thrust	Seconds Duration
65	Horizontal	A	2800	C + D C	633 440	49
66	Horizontal	A	2900	C + D C	633 438	26
67	Horizontal	A	3000	C + D C	633 440	23.5
68	Horizontal	B	3000	C + D C	633 438	27
69	Horizontal	B	2900	C + D	619 437	33
70	Horizontal	B	2800	C + D	634 444	29
71	Vertical	B	2800	C + D C	634 444	20.5
72	Vertical	B	2900	C + D C	634 444	38.5
73	Vertical	B	3000	C + D	629 445	38.5
74	Vertical	A	3000	C + D	629 438	42
75	Vertical	A	2900	C + D	627 444	41
76	Vertical	A	2800	C + D	629 444	41.5

* A = Aimed at edge of visible flame, 400-pound-thrust motor (between flames).
B = Aimed at center of visible flame, 400-pound-thrust motor (through flames).
C = "Lark" motor, acid-aniline, 400-pound-thrust.
D = "Lark" motor, acid-aniline, 220-pound-thrust.

[redacted]

Figure 5 - Bank of 1-ma pen recorders in mobile laboratory

Since the deviations in crystal current resulting from the flame barrier were small in comparison to the several possible errors in measurement, it was decided that only by a statistical analysis of the data could any useful values of energy redistribution due to the flame be obtained. Rather than burden the body of the report, the statistical method of treatment of the data, the errors considered, and the methods of calculating the error figures are detailed in an appendix for ready reference if such be necessary.

PRESENTATION OF DATA

Curves of the analyzed data (Figures 8-12, 14, and 15) show the deviation from the normal field pattern amplitude (in percent) plotted against the angle of the transmission path referred to the axis of the flame. The zero ordinate axis represents the "normal value" field pattern obtained without the flame or other barrier interposed in the radiation field. Thus, the curves show the degree of redistribution of field amplitude caused by the interposition of the flame or other designated barrier. A percentage scale is used because the observed effect for the flames was so small that decibel notation would be almost meaningless. For all curves, lines connect points representing the most probable values under the stated conditions. Where shaded areas are shown, they indicate the error region where, allowing for the calculated error, the true value is expected to lie. The boundaries of the shaded areas are determined by the error figure which is explained fully in the Appendix.

An accompanying curve (Figure 8) presents the data obtained from a single representative test run. This graph illustrates the low amplitude of the deviations compared to the expected experimental error and emphasizes the need for statistical treatment.

One-Motor vs. Two-Motor Condition

Figure 8 shows a rough comparison of the one-motor and two-motor conditions. Since other individual runs also showed distinct correlation between the one-motor and two-motor conditions it was decided to decrease the burden of analysis and plotting by treating further only the one-motor conditions which, on the whole, appeared to give more acceptable data. Since the radiation was directed primarily through the 400-pound-thrust motor flame, it was predicted that these two conditions would show strong correlation.

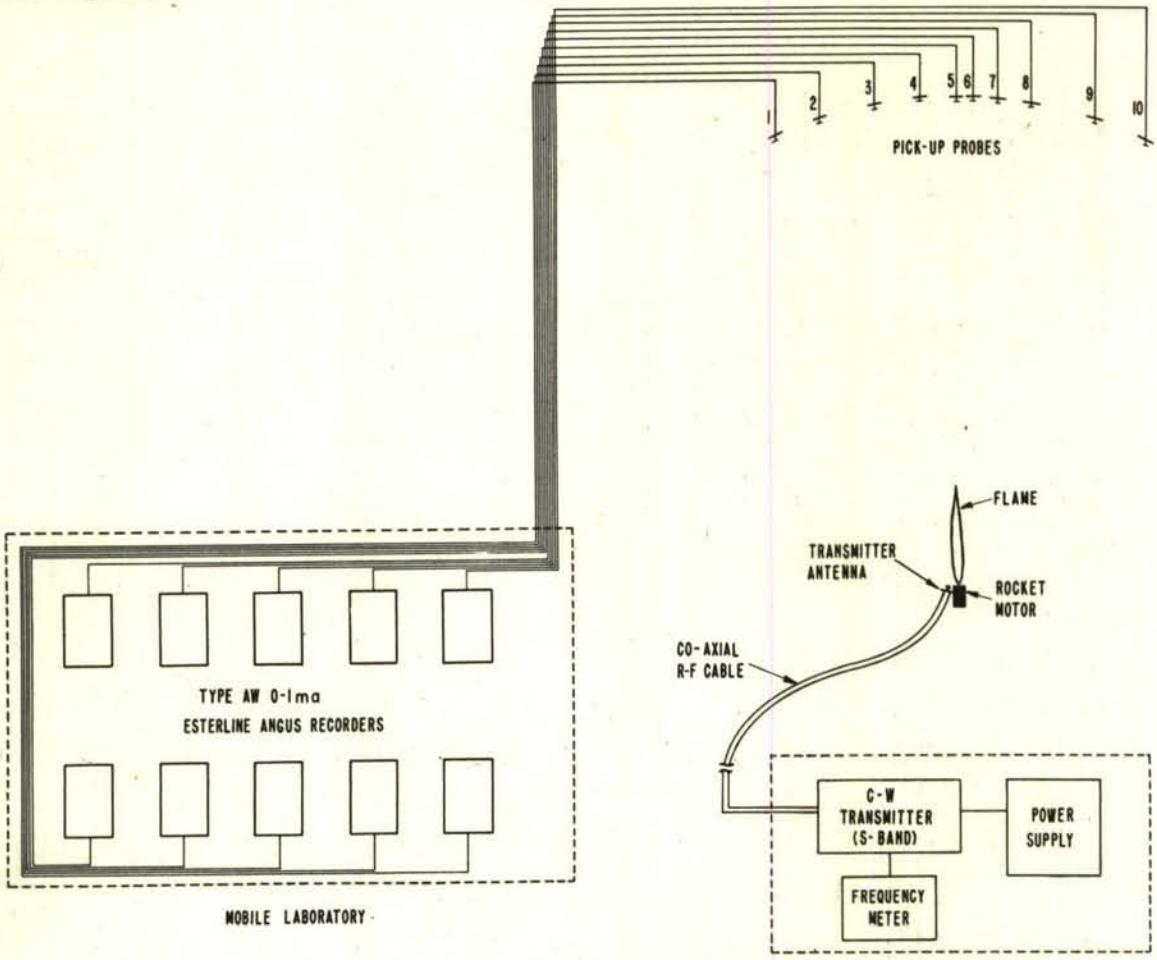

Figure 6 - Block diagram of instrumentation layout

Effect of Antenna Aim

The weighted averages of several measurement runs, with their expected error figures, are grouped for comparing the effect of aiming the radiation beam at the flame center against aiming at the flame edge (Figure 9). In addition to showing negligible departure between the values for these two aiming conditions, the plot shows the advantage in decreased error figure and smoother curves derived by the statistical averaging of the data. (Compare Figure 9 with that of Figure 8.)

For this study, the transmitting antenna was directed along two different vectors: Position A, on the line tangent to the uppermost edge of the visible portion of the 400-pound-thrust motor flame, and position B, in the plane of the pick-up dipoles and the central axis of the visible part of the same flame (Figures 1 and 2). For both positions the horizontal angle between the antenna axis and the flame axis was maintained at 10 degrees (Figure 4). The controlled variables frequency and plane of polarization were averaged together so as to accentuate only the effect due to the change in antenna aiming.

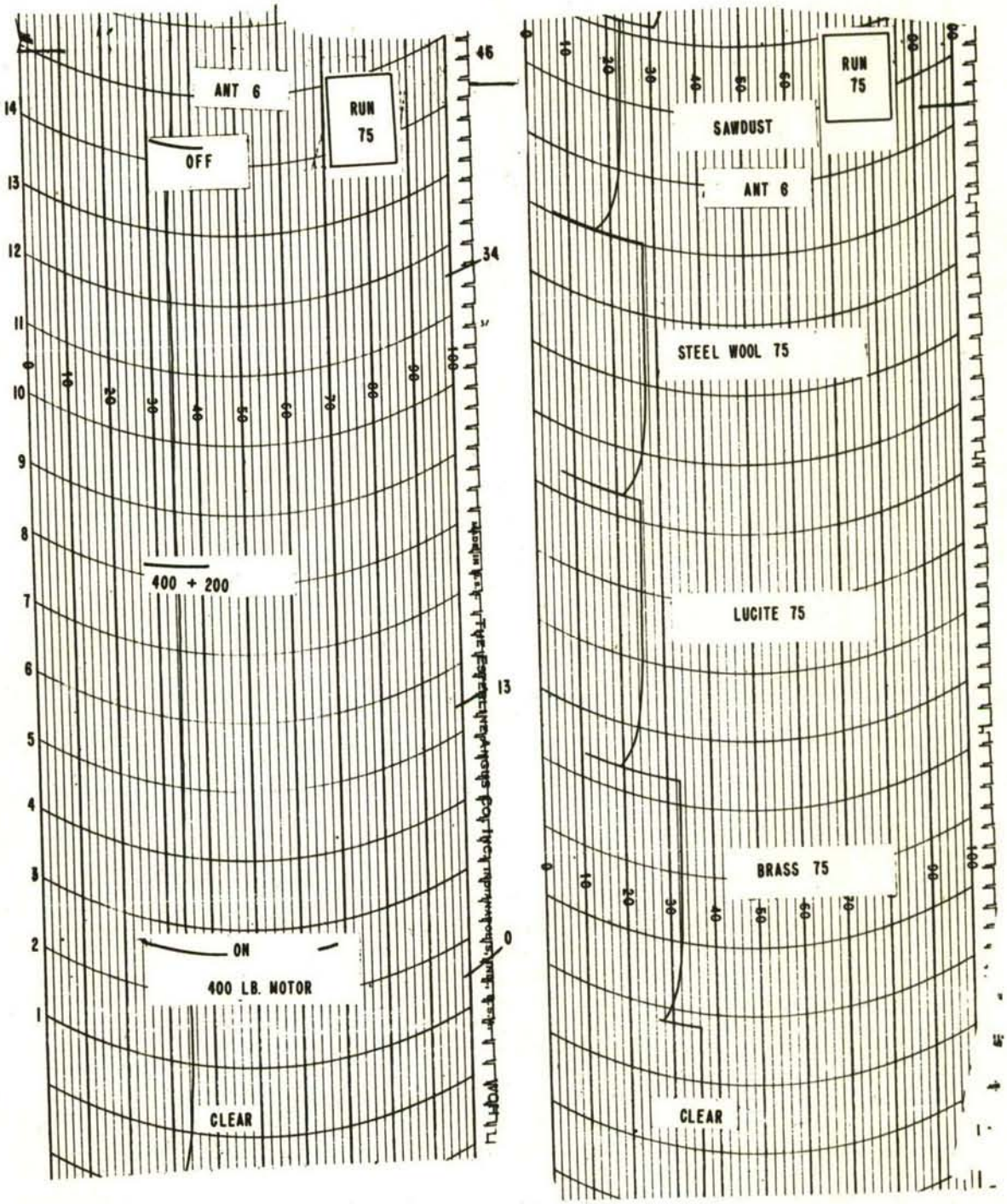

Figure 7 - Typical sections of chart paper (original data)

[redacted]

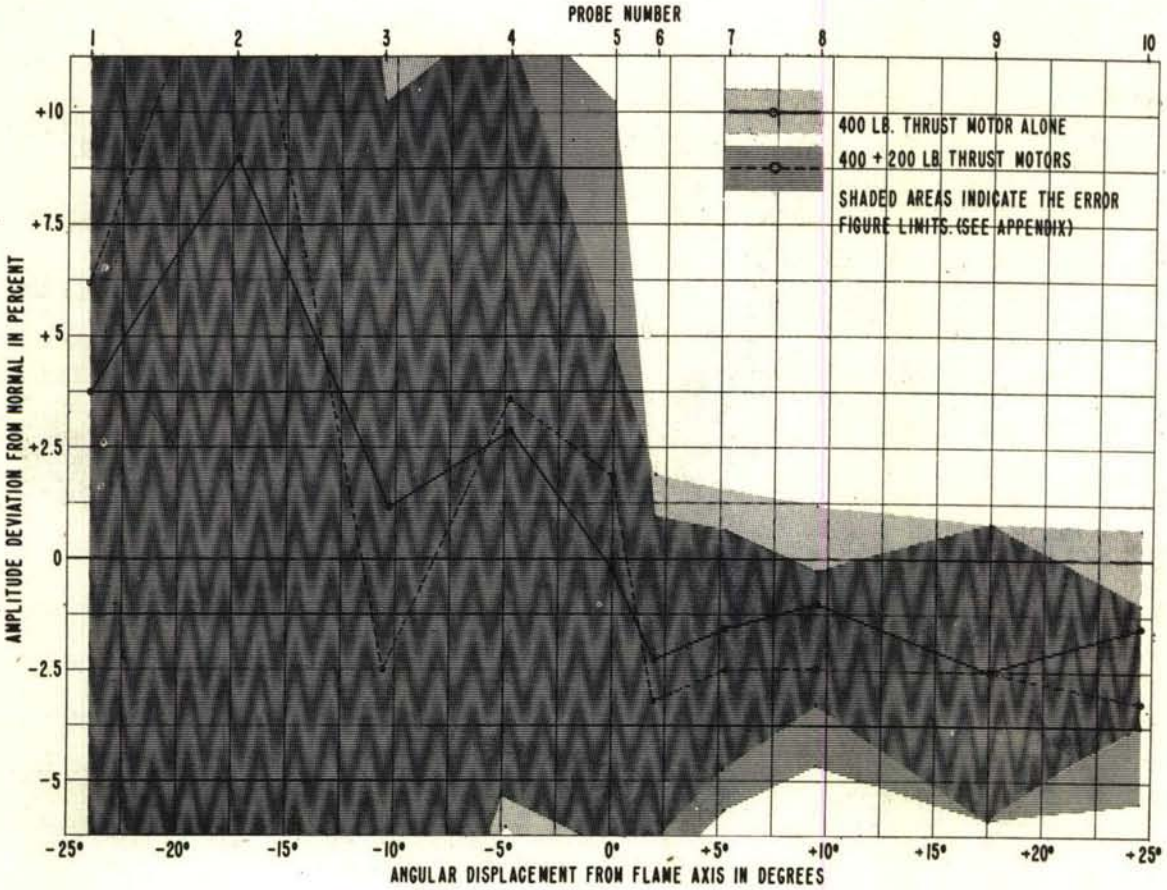

Figure 8 - Signal redistribution due to flame; representative test run (Run No. 75)

From the close proximity and similar trend of the two curves and the overlap of their error envelopes at all points (Figure 9) it may be concluded that under the stated conditions the point of beam incidence vertically on the flame is not critical and can be considered to have almost no effect upon the flame's apparent transparency to S-band radiation. This was to be expected since the slight change in antenna aim did not seriously change the radiation pattern at the pick-up probes. Only a strong refraction (bending around or away from the flame) would cause a significant difference in the percent-change figures.

Effect of Plane of Polarization

By changing the polarization plane of the transmitting antenna and probe pick-ups without altering their position, a comparison between horizontal- and vertical-polarization effects was obtained. Figure 10 shows the redistribution by the flame of horizontally and vertically polarized S-band radiation. The solid line and broken line represent the weighted averages of two groups of runs, denoting horizontal and vertical polarization conditions, respectively. The arbitrary error figures are presented as shaded areas about each curve.

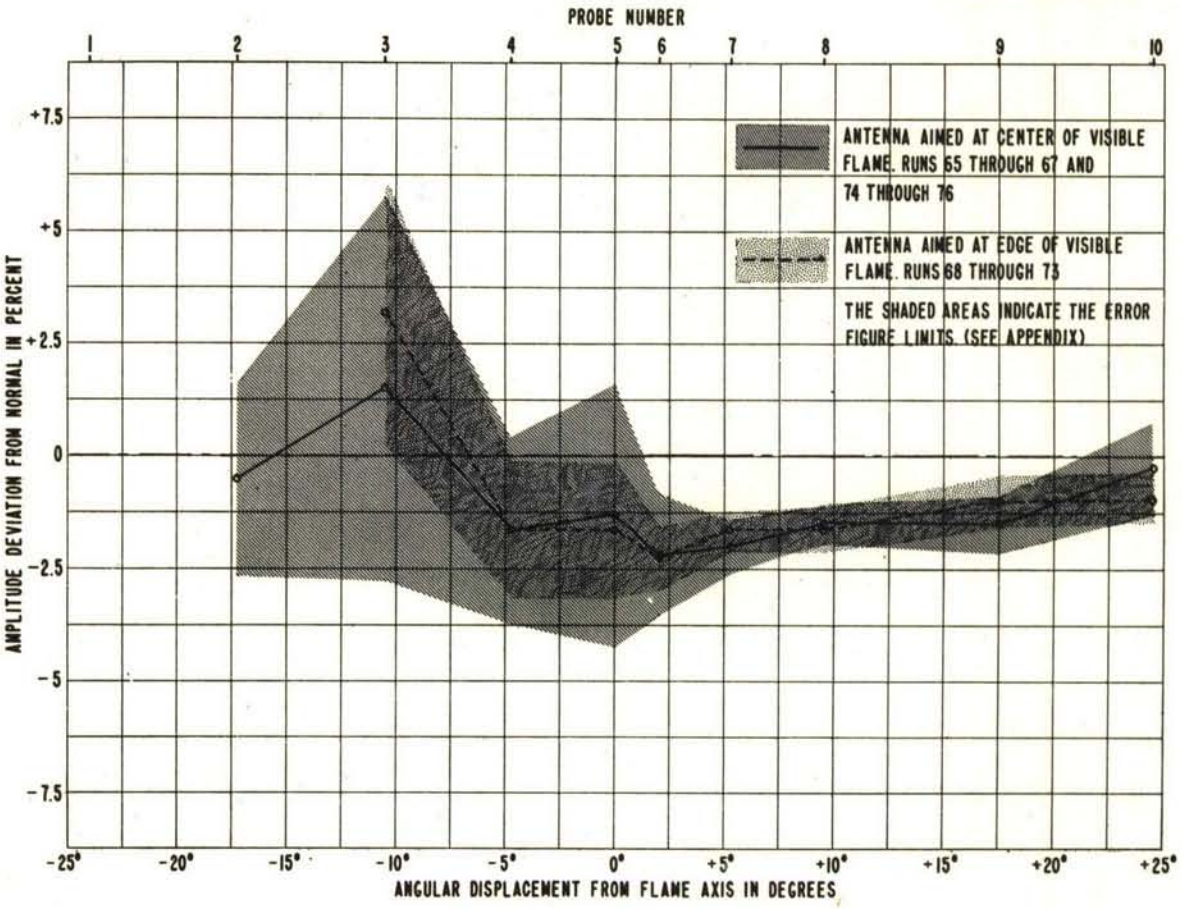

Figure 9 - Signal redistribution due to flame. Effect of aim point: Flame center versus flame edge

To simplify discussion of the curves, the arc of dipole pick-ups has been arbitrarily divided into three sections or regions (Figure 4). Region I covers the arc section -25 degrees to -5 degrees. In this region signal redistribution due to reflections from the flame should be apparent, if present. Unfortunately, this is the region of least signal, and thus of decreased accuracy. Region II, about the flame axis, covers -5 degrees to +5 degrees of the arc and covers the area where the signal transmission path intersects the flickering end of the flame. Refraction effects, especially any bending toward the flame axis, should be detectable in this region, if present. Region III, from +5 degrees to +25 degrees of the arc, covers the area of through- and cross-flame transmission paths where the actual path length within the flame decreases with increasing angle.

In Region III one finds that the two weighted-average curves lie within the overlap of their error figures. Thus, under cross-flame conditions it is shown rather conclusively that polarization has negligible effect on the redistribution of the S-band radiation. In Region II, the flame appears to be more transparent to the horizontally polarized signal. This phenomenon, if indeed real, would be difficult to explain unless there existed a tendency by the vertically polarized signal to be bent away from the flame axis. It should be noted in this connection, however, that the displacement represents only a fraction of a decibel change in the received signal amplitude, and also that the error envelopes overlap

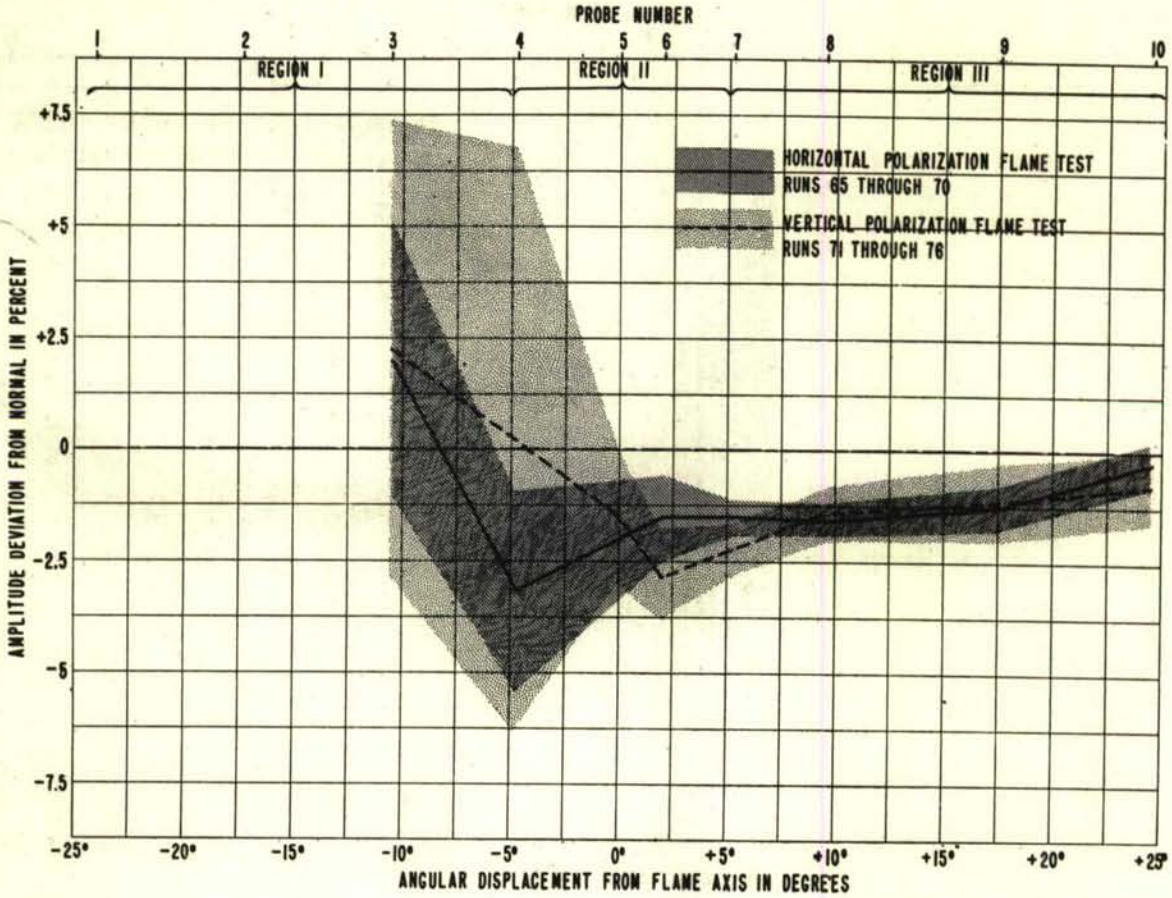

Figure 10 - Signal redistribution due to flame; horizontal versus vertical polarization

slightly. In Region I the higher error figures tend to mask any observable effects, although some displacement is evident.

Ground reflections may have played a part in these results. Since the antenna and pick-up positions were not changed at any time with respect to the ground, any error from this source should at least be a constant one, resulting only in a fixed dilution of the signal. An exception would be the comparison of horizontal and vertical polarizations where it would be expected that the horizontally polarized signal would be reflected from the ground to a far greater degree than the vertically polarized signal.

Since the curves representing the two polarization conditions (Figure 10) lie, on the whole, much closer to each other than to the "normal" or "zero" line, it can be assumed that deviation due to the effect of ground reflection is certainly less than the deviation due to the interposition of the flame. However, small changes in the phase angle of the arriving ground-reflected wave, due to the uneven character of the ground and slight variations in path length, might account for the deviations shown by the polarization curves.

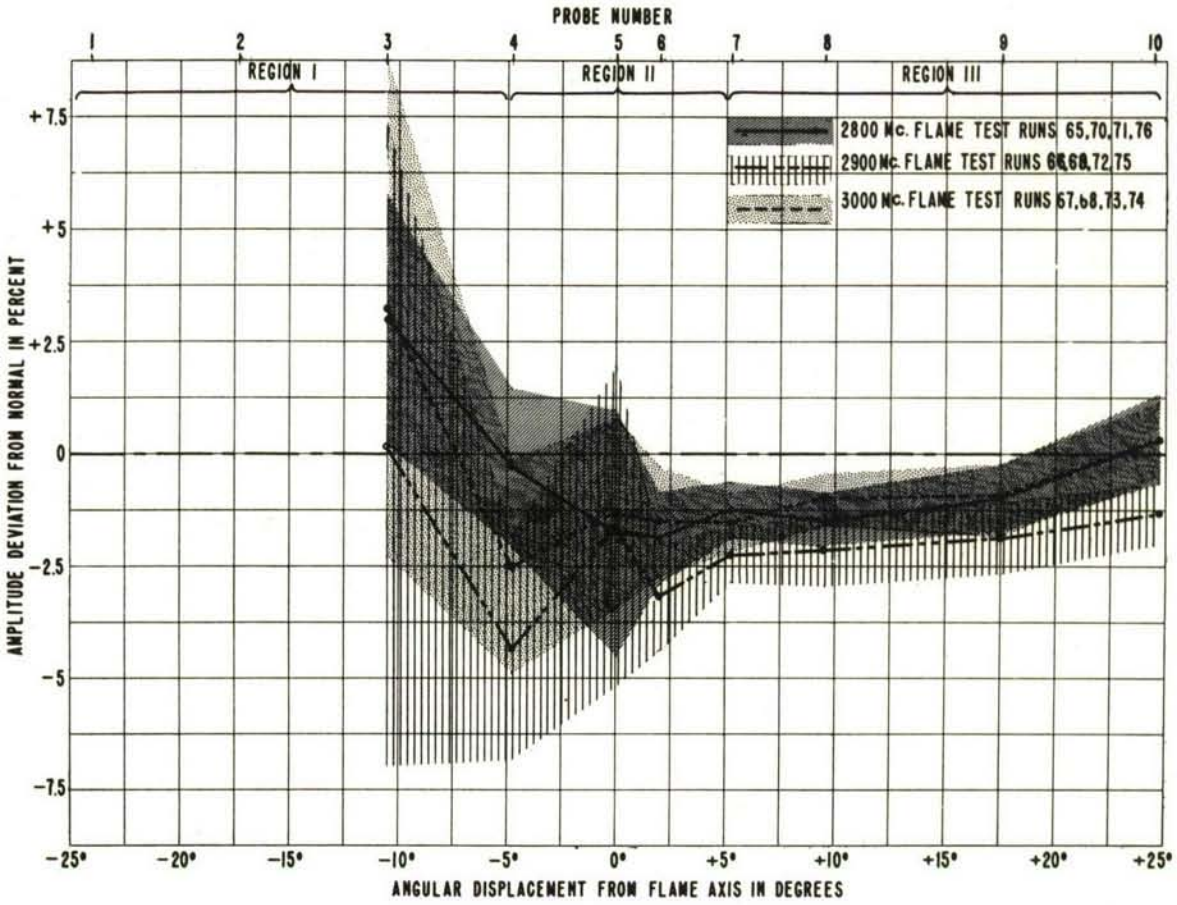

Figure 11 - Signal redistribution due to flame; effect of frequency variation

Effect of Frequency Variation Within Upper S-Band

With the measurement setup unchanged, data was obtained at three different frequencies within the S-band: 2800 Mc, 2900 Mc, and 3000 Mc. In Figure 11, all variables other than frequency have been statistically treated together. The three heavy lines are the weighted averages, one for each specified frequency. As before, the shaded areas represent error envelopes of the data obtained at each frequency. It should be noted that although three distinct curves were obtained, one for each frequency, they all follow the same general trend.

In Region III of Figure 11 the order of the weighted average curves is always the same, being 3000 Mc, 2800 Mc, and 2900 Mc in order of effective insertion loss through the flame. Although the overlap of error figures indicates that the separation between these curves is not positively real, probability suggests a definite separation for the 2900 Mc curve at least. There is a strong possibility that the differences observed are due, at least in part, to interference between the direct and ground-reflection paths, since rough calculations show that a phase difference of at least $\frac{\pi}{10}$ should be expected between paths in changing from one frequency to the next.

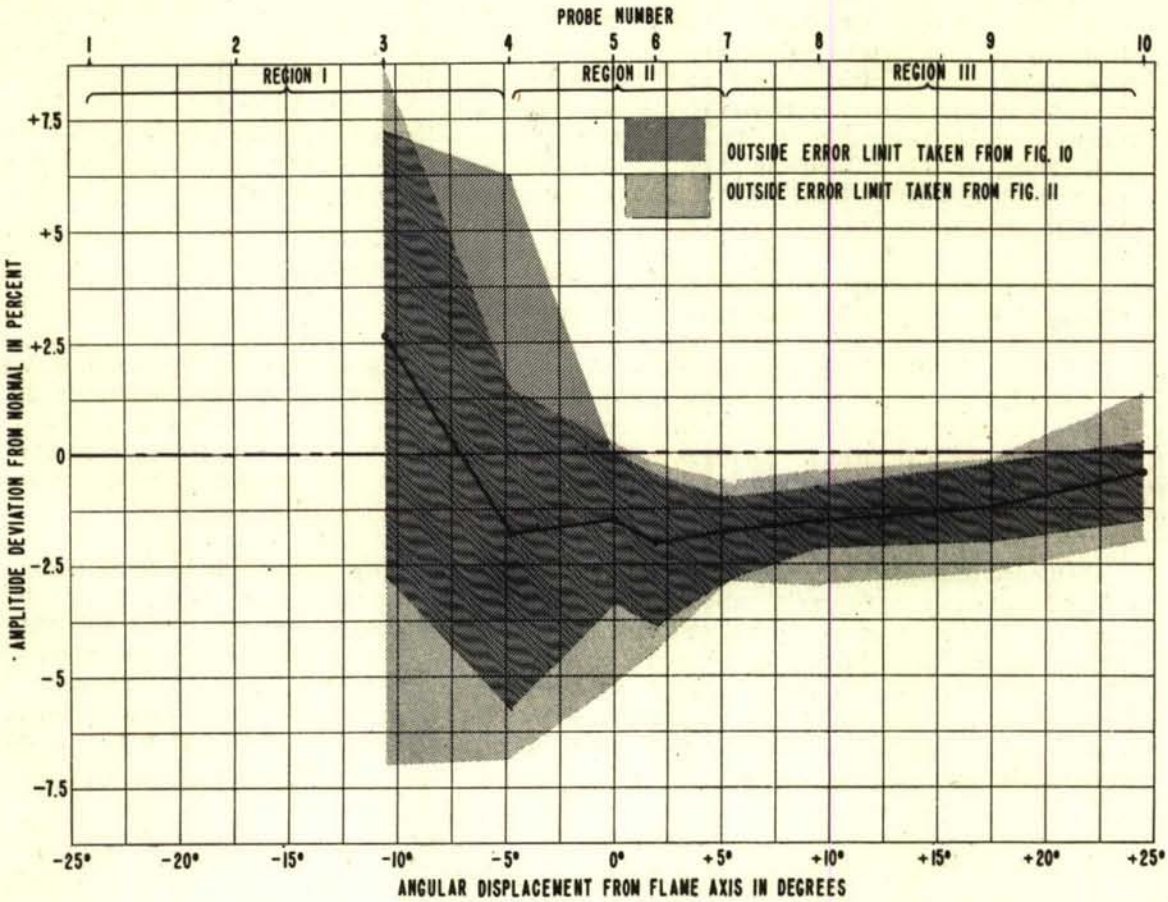

Figure 12 - Signal redistribution due to flame; general mean curve for all runs

In Region II of Figure 11 the weighted average curves cross over but the error envelopes remain overlapped, indicating no significant difference from Region III. The error figures are so high in Region I that the data is inconclusive, but at least the magnitudes involved do not seem to be out of line. In this region, small phase differences between the direct and any flame-reflected ray due to frequency changes should become evident as a further separation of the curves.

Over-All Effect of the Flame Upon S-Band Radiation

To make a clearer picture of the over-all effect of the flame upon S-band radiation, the data contained in Figures 10 and 11 were weighted and averaged. By averaging out at least part of any frequency and polarization effects a practical mean value for the flame insertion effect may be obtained. This weighted average gives a single curve (Figure 12) showing the general mean of all the data. Since the computation of a propagated error is not applicable in this case, the combined error envelope limits of Figures 10 and 11 are indicated by the shaded areas.

Figure 12 reveals that in the region between pick-up dipoles Nos. 6 and 9, the redistribution of the S-band radiation due to the flame creates an apparent insertion loss of from 1.5 percent at pick-up dipole No. 6 (+2 degrees from flame axis) to 1.25 percent at pick-up dipole No. 9 (+17.5 degrees from flame axis). Since the error figures in this region are always below the axis, the redistribution of energy is definitely negative. This means that the flame is effectively an insertion loss although the values of this insertion loss cannot be determined exactly. From Figure 4 it may be observed that the region between pick-up dipoles Nos. 5 and 9 is that in which the detected radiation passes down through the flame.

The gradual slope of the general mean curve (Figure 12) between pick-up Nos. 6 and 10 appears to be directly related to the radiation path length within the flame (Figure 4).

The slight irregularity of the general mean curve between pick-up dipoles Nos. 4 and 6, (Region II) is difficult to explain. However, it is important to note that these pick-up dipoles cover the radiation paths intersecting the end of the visible flame where it becomes fluttery and diffuse. Quite possibly then, small irregularities in this region and perhaps elsewhere in the curves are due to imperfect alignment of the individual transmission paths exactly through the flame axis.

The fact that the general mean curve increases sharply between pick-up dipoles Nos. 4 and 3 and crosses the axis indicates that the redistribution of S-band radiation in this region (-4.75 degrees to -10.5 degrees from flame axis) resembles reflection from the flame. From Figure 4 it may be seen that this is the region in which reflection of the radiated energy from the flame would be most pronounced. Unfortunately, the error envelope in this region is so large that positive statements should not be made. The large error envelope associated with data obtained from pick-up dipoles Nos. 1 and 2 was so objectionable that the data was ignored.

Flame vs. Artificial Barriers

Artificial barriers of sawdust,[6] steel wool,[7] lucite,[8] and brass[9]—all physically smaller than the visible portion of the 400-pound-thrust motor flame—were substituted for the flame and placed in the flame position as shown in Figure 13. This was done to determine the relative effect each one might have upon the redistribution of the S-band radiation as compared with the flame itself. Figure 14 contains a weighted mean curve (similar to Figure 12 but at a different scale, and for runs 73, 74, 75 and 76 only) and a curve obtained by taking the arithmetical mean of the data obtained when the flame was replaced by a lucite[8] barrier.

The general trend of the redistribution of energy caused by the lucite barrier is the same as that obtained with the flame. However, the amplitudes of the redistributed energy levels due to the flame were secondary in comparison to those obtained when the flame was replaced by the lucite barrier. In general, at S-band a lucite tube as used here is not considered an appreciable reflector.

---

[6] 1/4-inch cardboard tube approximately 3 inches o.d. x 36 inches filled with dry sawdust.

[7] Tight roll of medium steel wool approximately 3 inches o.d. x 36 inches wrapped to form with kraft paper.

[8] 1/8-inch lucite tube 3 inches o.d. x 36 inches.

[9] Brass telescopic tubing approximately 3 inches o.d. x 36 inches.

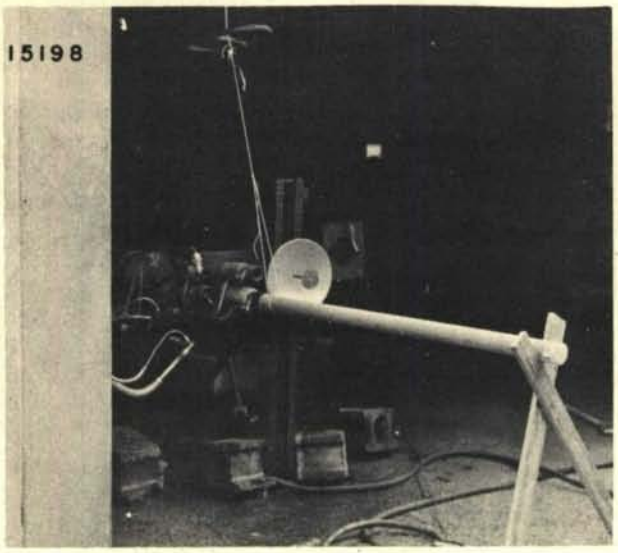

Figure 13 - Artificial barrier in position

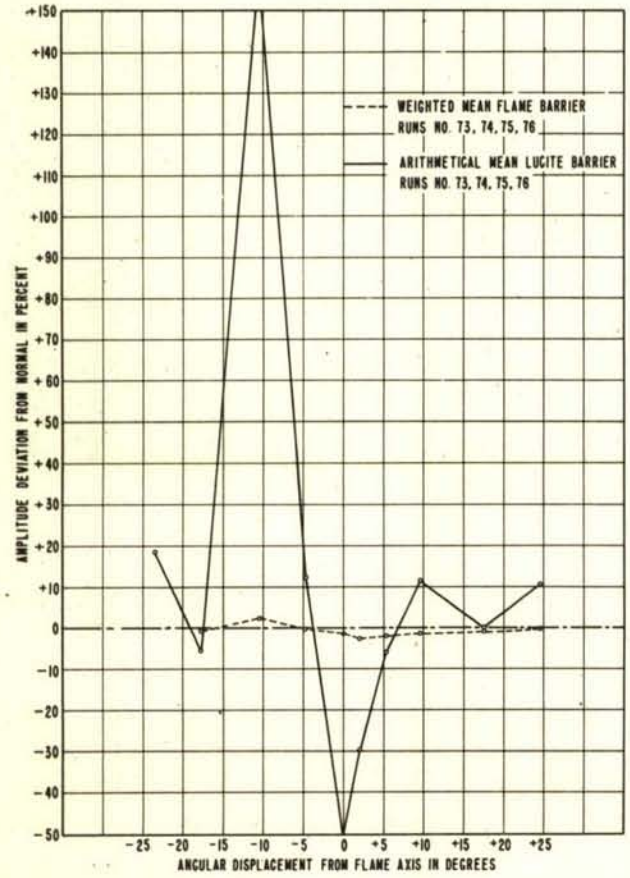

Figure 14 - Signal redistribution due to flame compared with that due to lucite barrier

Figure 15, which is divided into four plots, contains the data obtained when the flame was replaced with artificial barriers. Tests were conducted at three frequencies within S-band for each barrier as indicated on the plots. Attention is drawn to the fact that the scale of the amplitude deviation from the normal on Figure 15 is considerably compressed when compared to the plots (Figures 9, 10, 11, and 12) showing the results of the flame studies. The general trend of the data obtained is the same for all of the barriers at the frequencies employed. The effects of changing the frequency within upper S-band were random and can be explained by multipath changes in phase relationships. Conductors (brass), absorbers (steel wool), poor conductors (sawdust), and nonconductors (lucite), when introduced independently as barriers, gave similar effects upon the redistribution of the S-band radiation. Due to alignment problems and the narrowness of the barriers it is not certain that they completely intercepted the radiation paths. Because of this and the presence of ground-reflection paths it is expected that the indicated attenuation values are less than they should be.

CONCLUSIONS

On the basis of the data presented in this report, the following general conclusions on the propagation of S-band radiation through acid-aniline flames have been derived:

(a) In general, the phenomena observed can be most easily explained in terms of redistribution of the transmitted energy due to the flame acting as a partial reflector and partial absorber.

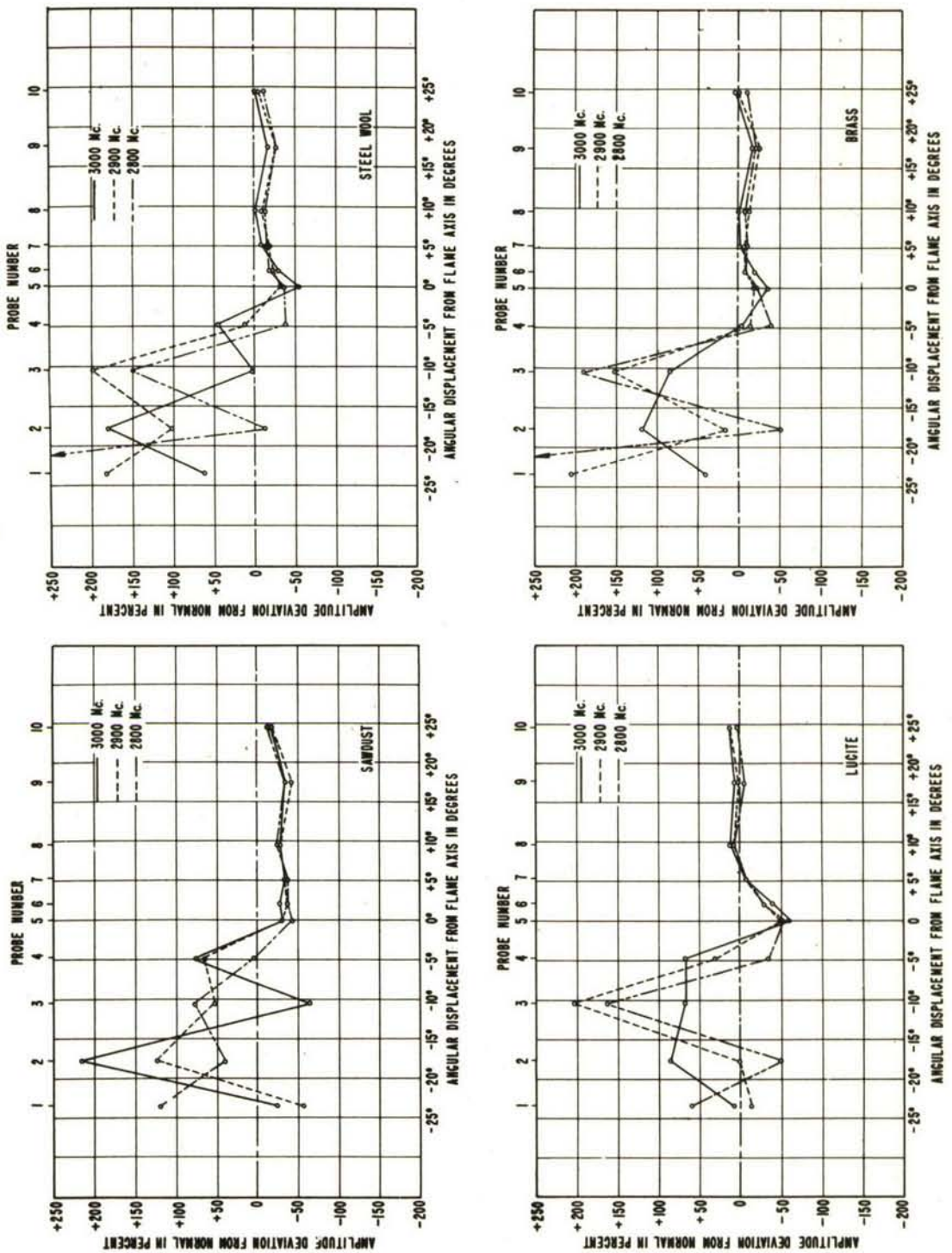

Figure 15 - Signal redistribution due to artificial barriers at 3 S-band frequencies

[redacted]

(b) The redistribution of S-band energy directed at the 400-pound-thrust motor flame was substantially the same in the single-motor condition as that due to the combined flames of the 400-pound-thrust and 200-pound-thrust motors.

(c) Polarization of the S-band radiation has no noticeable effect upon the apparent transparency of the flame to S-band radiation passing through and across the flame.

(d) The redistribution of the S-band radiation directed across the flame showed a decrease of from 1.25 to 1.5 percent (less than 0.1 db) from the normal value. However, since all the energy did not pass directly through the flame area, the attenuation indicated is slightly less than the true value. Instrumentation now under development is expected in future experiments to more accurately determine small attenuation figures as well as to provide for precise measurement of large values.

(e) Increasing the in-flame length of the radiation path traversed causes increasing insertion loss.

(f) The slight random change in energy redistribution noted when the frequency was changed in steps of 100 Mc can be accounted for by partial phase addition and subtraction due to multipaths.

(g) The general trend of the redistribution of energy caused by the flame was roughly paralleled by that obtained when using a lucite tube barrier in place of the flame. However, the amplitudes of the redistributed energy levels due to the flame were secondary when compared to that obtained with the lucite barrier.

ACKNOWLEDGMENTS

The authors wish to make acknowledgment to NRL scientists, F. Malcolm Gager, Frank E. Boyd, J. M. Headrick, W. J. J. Klein, Gerald D. Morehouse, Ralph O. Parker, and Frederick E. Wyman, who were members of the field party at the Test Area of Reaction Motors, Inc., in June 1947. They spent long hours setting up and operating the complicated instrumentation under the various rocket flame conditions. Mention must also be made of the continuing aid in the lengthy process of data reduction by Miss Ethel Smith, Mr. Henry Ray, and Mr. John Adams, all of the Special Research Branch, Radio Division III, NRL.

* * *

APPENDIX
Discussion of Analytical Method

BASIS OF ANALYSIS

Since methodical analysis of the experimental data on a statistical basis was followed for this report, a brief discussion of the methods used and errors involved is pertinent. The methods used were dictated by the form of the experimental data collected and not by pre-test planning. Experimental difficulties, plus the fact that the flame was far more transparent than anticipated, resulted in data where the desired information was of the same order of magnitude as the errors involved. An effort was made to abstract as much information as possible from each group of data by averaging like runs and thereby averaging out some of the error (cf. increasing the signal-to-noise ratio in an electronic system by integrating a repetitive signal with time).

ERROR SOURCES

Listed below are the likely instrument error sources and their evaluation.

Signal Source (Magnetron Oscillator and Antenna Link)

Frequency Drift - Assuming no resonant effects, the likely frequency drift (.1% or .2%) causes errors of a secondary nature only.

Amplitude Drift - This error source is due to drift in the power output of the magnetron oscillator because of temperature effects, tube aging, frequency drift, and other factors. It is a considerable error source but its effect is reduced by suitable corrections.

Vibration Effects, Modulation, Etc. - Although the S-band signal source was fairly well insulated from the vibration field and used well filtered power supplies, some microphonics and hum modulation were present (estimated 5% modulation). The power-source hum was constant, so did not effect the results. The contribution to the results by microphonic effects at the signal source was considered negligible after a check run with the transmission path not directed through the flame showed no effective deviation.

Detector (Silicon Crystal Probe)

Nonlinearity - The rectification characteristic of the silicon crystals used (type 1N21) follows a rough "square-law" and so departs from linearity, especially at low field strengths. A study of average crystal curves for the frequencies used, however, shows that for crystal currents above 0.1 ma the curve is substantially linear with field strength, at least over the range of variation involved in the flame tests. Corrections were made when necessary.

Drift in Efficiency of Crystal - It was found that aging effects, including heat and vibration, slowly changed the activity of the crystals used. Crystals were replaced when activity was noticeably low and corrections were made to compensate for drifts detectable during a run.

Vibration Effects - The crystals used were subject to a high vibration field and certain crystals behaved erratically during a run. This erratic element was partially compensated for by averaging several readings during a run and by including in the overall error figure an element roughly proportional to the erratic behavior shown by a particular crystal.

Recorder (Esterline-Angus, 1 ma Movement)

Horizontal Paper Alignment - The recording chart paper has a tendency to wobble from side to side as it is drawn through the rolls. This is due to the clearance allowed in the punched holes, play in the roll bearings, and misalignment of the rolls. This error varies from one instrument to the next.

Index - The index lines printed on the recording chart paper are not perfectly uniform. This error is assumed negligible when compared to the error mentioned above.

Pen Bounce - When the instrument is subjected to vibration, or when the paper is moved irregularly (as when writing into the record while in operation), the pen sometimes jounces on the paper causing an error. This error is usually erratic and random in effect.

Pen Friction - Particularly when not in exact balance, the E-A recording pen, by frictional contact with the paper, tends to hold its previous position when a slight change in input is not sufficient to overcome the horizontal friction component. This error is essentially constant and likely to occur equally in a positive or negative direction.

Pen Lag - The inertia of the moving pen system causes a time lag before a sudden change in input is fully indicated by the record. This time lag is in the neighborhood of 2 seconds and can be essentially eliminated by reading at successive time intervals greater than 2 seconds, assuming the run-time is of sufficient length.

Speed Irregularity - Especially when the spring motor is running down, the paper tape often moves jerkily, resulting in uneven timing. Synchronizing time marks were recorded on each tape to check this error. Examination of the records revealed that the irregularity was not serious and could be neglected when 3 or more time lines (cross-lines) were used for averaging over each operational phase.

Meter Movement - Although the meter movements of the recorders were probably not off in accuracy more than 2%, this error was assumed constant throughout the tests and was considered negligible over the small variations noted.

Zero Index - The recorder is equipped with a manually operated zero index to correct for minor alignment errors. This zero index was carefully checked and adjusted when necessary before each run. Errors from this source were very small and were ignored.

Flame

Starting and Stopping Transients - As it was expected, the popping and wheezing of the flame during starting and stopping caused erratic indications on the record. Only data collected during steady-state conditions of the flame were used.

Steady-State Variations - The motor charts of each run were scanned, especially the thrust plots. The runs were found to be quite uniform in thrust in the steady-state condition. Small variations during a single run were minimized by averaging over the whole steady-state time.

Treatment of Data

By utilizing relative information (percent-difference between flame-on and flame-off values) and not absolute readings (field strength), corrections for antenna patterns were by-passed directly. This also enabled better comparisons between runs since small changes in the power level of the source between runs could be neglected. The data from each pick-up probe for each run consists of a signal-level versus time plot from an Esterline-Angus 0-1.0 ma recorder, the time beginning about fifteen seconds before the flame is started and ending about fifteen seconds after the flame is extinguished. Reduction of this data is accomplished by suitable averaging and smoothing of the before- and after-flame values. The difference is then calculated and expressed as a percentage of the flame-off value. Error figures are estimated to indicate the relative merit of each percentage value.

Smoothed values are obtained from the charts by the method detailed below:

(a) Each chart is divided into seven sectors along the time axis to represent the following phases in order: (1) Before-flame; (2) flame-starting transients; (3) single-flame operating; (4) second-flame starting transients; (5) both flames operating; (6) flame-stopping transients; (7) after-flame. The boundary lines are positioned by reference to the photo-cell monitoring records and by checking against the timing pulses, the recorded transient phenomena, notations and sync markings on the chart, and by comparison with the motor-thrust charts.

(b) The sectors enclosing the transient phenomena are now forgotten. Equal time lines as printed on the chart paper (every five seconds) are chosen to mark arbitrary time intervals. These lines are now numbered consecutively (1, 2, 3, etc.) when they lie within each of the data sectors: A, before-flame; B, single-flame operating; C, both flames operating; D, after-flame.

(c) Smoothed values are read and recorded from the chart to the nearest two-hundredth-full-scale divisional part (.005 ma) for each numbered line. (Values are mentally smoothed over the distance $\pm$ 1/2 time division from each time line.)

(d) The arithmetical mean is computed from the time-spaced values for each data sector. These mean values are labeled M_A, M_B, M_C, and M_D, respectively. All data from any probe for any particular run netting a mean flame-off value (M_A) less than 0.1 ma are arbitrarily discarded since the reading error would be far greater than the percentage-change value.

(e) The percentage change for data sectors B, C, and D are computed with respect to A:

$$P_B = \frac{M_B - M_A}{M_A} 100,\ P_C = \frac{M_C - M_A}{M_A} 100,\ P_D = \frac{M_D - M_A}{M_A} 100.$$

(f) For each run, an arithmetic mean is determined of the after-flame percentage-change values (P_D) for all probes (excepting those eliminated in step "e" above; in this case, probes 1 and 2):

$$\overline{P_D} = \frac{P_{D3} + P_{D4} + P_{D5} + - - - + P_{D10}}{8}.$$

This is the mean drift error for each run.

(g) Mean time values for each data sector are determined for each run by counting the total time lines on the data chart and obtaining the mean time value for each data sector. These mean time values are then adjusted to make the mean time value for sector A equal to zero. The resulting times are then $T_A = 0$, T_B, T_C, and T_D.

Drift corrections are obtained separately for each run and operational phase as follows:

$$Q_B = \frac{\overline{P_D}\, T_B}{T_D},\ Q_C = \frac{\overline{P_D}\, T_C}{T_D}.$$

Corrected percentage-change values for each run are found by using the applicable drift correction:

$$\overline{P_B} = P_B + Q_B,\ \overline{P_C} = P_C + Q_C.$$

These $\overline{P}$ values are used as the best first approximation of real values for each run.

COMPUTATION OF ERROR FIGURE

A figure of merit for each probe for each run is estimated in the form of an arbitrary error figure, e, which represents a likely range of departure from the true value. This error figure is formed by statistical addition of a lumped reading error and a figure giving a rough estimate of the crystal detector instability.

After careful analysis of the recorder errors listed under "Error Sources" it was decided to lump the recording instrument errors, allowing $\pm$ .007 ma as the probable error for all instruments for all runs. This figure, expressed as a percentage change, $e_b = \frac{0.7}{M_A}$, checks out well in practice. The probable error of the more or less erratic crystals is taken to be the after-flame percentage-change value corrected for drift $e_C = P_D - \overline{P_D}$ for a particular run, or $\overline{e_C} = .6745\sqrt{\frac{\Sigma_o^n e_C^2}{n}}$, averaged over several runs which ever is greater. This error figure may seem unnecessarily severe but it is desired to reduce as far as possible the chance that crystal erraticity might be reflected in the results.

[redacted]

The arbitrary error figure, e, for each probe and run is then calculated as: $e = \sqrt{e_B^2 + e_C^2}$ expressed as a percent value. Probe readings where e exceeds 15% are eliminated at this point.

WEIGHTED AVERAGES

By combining values from several runs along with their error figures, mean values were obtained with a considerable improvement in error figure. In an effort to obtain the best possible values, weighted averages were used so that probes and runs which, because of high signal level or nonerratic crystals, were inherently less in error could be given the most credence. Standard statistical practice is used in proportioning the weights to the inverse square of the error value:

$$W = \frac{100}{e^2} .$$

The resulting weighted mean is then:

$$\bar{P}^1 = \frac{\Sigma(\bar{P} \times W)}{\Sigma \quad W} .$$

PROPAGATION OF ERRORS

The statistical propagated error is determined by taking the geometric mean of the weighted errors:

$$E = \sqrt{\Sigma\left(\frac{E \times W}{\Sigma W}\right)^2} .$$

As a final check, residual errors (e_r) are also computed: $e_r = \bar{P}^1 - \bar{P}$.

The standard deviation, $\sigma = .6745\sqrt{\Sigma(e_r)^2}$, is then calculated and compared with E, above. In plotting combined results of more than one run, the larger of the two final errors, E and σ, is used as the arbitrary error figure to indicate the probable range of deviation of the true value from the best statistical value.

The methods used herein constitute an intuitive adaptation of standard methods to the peculiar set of data at hand. The significance which can be given to the final error figure is that it locates the region wherein there is a high probability of the true value resting.

* * *

[redacted]